Electromagnetic scattering from two-layered rough interfaces with a PEC object: vertical polarization*

Wang An-Qi(王安琪)†, Guo Li-Xin(郭立新), and Chai Cao(柴 草)

School of Science, Xidian University, Xi'an 710071, *China*

(Received 7 July 2010; revised manuscript received 17 January 2011)

Electromagnetic (EM) scattering from a stack of two rough interfaces separating a homogeneous medium with a perfectly electric conducting (PEC) object has been calculated through the method of moments for vertical polarization. Theoretical formulations of EM scattering from multi-layered rough interfaces with a PEC object have been derived in detail and the total fields and their normal derivatives on the rough interfaces are solved. The two-layered model is a special case. In this work, a Gaussian rough surface was applied to simulate the rough interface. A cylinder was located above, between or below the two-layered rough interfaces. Through numerical simulations, the validity of this work is demonstrated by comparing it with existing scattering models, which are special cases that include a PEC object located above/below a single-layered rough interface and two-layered rough interfaces without an object. Subsequently, the influences of characteristic parameters, such as the relative permittivity of the medium, as well as the average height between the two rough surfaces, on the bistatic scattering coefficient are discussed.

Keywords: composite scattering, two-layered rough interfaces, electromagnetic wave scattering, method of moments

PACS: 02.60.Jh, 41.20.Jb, 43.30.Hw **DOI:** 10.1088/1674-1056/20/5/050202

1. Introduction

Electromagnetic (EM) scattering from layered rough interfaces with/without an object has been extensively investigated for various applications, including landmine, pipe or other buried object detection, and depth measurement of snow-covered earth or of oil covering an ocean surface.[1−3] Approximate analytical methods, such as the Kirchhoff approximation [1] and the small perturbation method,[2] have been applied to investigate the properties of EM scattering from two-layered rough interfaces. However, those two analytical methods have strict limitations, low precision and are not effective for computing composite scattering from two-layered rough interfaces with an object. The finite difference time domain (FDTD) technique has been presented to compute bistatic scattering from an object above a two-layered rough interface.[3] The extended boundary condition method and the scattering matrix technique have been used to study EM scattering from layered rough surfaces with and without a cylinder buried in it.[4,5] Unlike these methods, the method of moments (MOM) achieves a high level of accuracy by directly applying the boundary conditions on the interfaces. Based on the MOM, the propagation inside layer expansion (PILE) method is combined with the banded matrix iterative approach canonical grid method, or forward-backward spectral acceleration, to calculate EM scattering from a two-layered rough surface with an object.[6−8] In this work, the theoretical formulations of EM scattering from multi-layered rough interfaces under vertical (VV) polarization are provided, the total fields and their normal derivatives on the rough interfaces are solved. The two-layered model is a special case. Significant improvements to the integral equations and the matrix equation are also presented for when an object is located above or below the multi-rough interfaces or between any two rough interfaces. The purpose of this work is to combine the accuracy and validity of integral equations and matrix equations to calculate EM scattering from multi-layered rough interfaces with or without an object. Detailed derivations are described based on the previous work[9−13] of our research teams. The MOM algorithm with the pulse basis function and the point

*Project supported by the National Natural Science Foundation of China (Grant No. 60971067), the Specialized Research Fund for the Doctoral Program of Higher Education, China (Grant No. 20100203110016), and the Fundamental Research Funds for the Central Universities, China (Grant No. K50510070001).

†Corresponding author. E-mail: wanganqi0006@163.com

© 2011 Chinese Physical Society and IOP Publishing Ltd

matching technique[14,15] is proposed to compute EM scattering from two-layered rough interfaces. The biconjugate gradient method (BICGM)[16] is introduced to reduce the iterative process of solving the unsymmetrical matrix equations.

In this work, a Gaussian rough surface is applied to simulate a realistic rough interface. It is generated through the Monte Carlo method and is truncated into finite length. The incident wave cannot be simply chosen as a plane wave and should be expressed as a tapered plane wave in which energy is distributed in a narrow beam for the mean incident angle. In this study, the tapered plane wave suggested by Thorsos,[17] which satisfies the requirement and the Maxwell's equation in an appropriate sense, is regarded as the incident wave. The validity of this paper is shown by comparing it with existing scattering models, which are special cases that include a perfectly electric conducting (PEC) object located above/below a single-layered rough surface[18] and a two-layered rough surface without an object.[6]

This paper is organized as follows. In Section 2, the geometric model of this scattering problem, the derivations of the integral equations and the matrix equations are described in detail. In Section 3, several numerical simulations are presented. The influences of characteristic parameters, such as the relative permittivity of the mediums, as well as the average height between the two rough surfaces on the bistatic scattering coefficient (BSC), are discussed. Section 4 provides a summary and a proposition about further investigation of this topic.

2. Theoretical formulations

A VV polarized wave $\psi^{\rm inc}(\boldsymbol{r})$ is assumed to be impinging upon a geometric model, as shown in Fig. 1, where the P layered rough surfaces are independent of each other. The surface height profiles are denoted by $z = f_p(x)$ $(p = 1, 2, \ldots, P)$, where $f_p(x)$ is a Gaussian process with a height Gaussian spectrum and satisfies $\langle f_p(x)\rangle = -d_p$. Here, $d_1 = 0$. In Fig. 1, $\theta_{\rm i}$ and $\theta_{\rm s}$ represent the incident angle and the scattered angle, respectively. Spaces Ω_p $(p = 0, 1, \ldots, P)$ are filled by a homogeneous medium with relative permittivity ε_p $(p = 0, 1, \ldots, P)$, in which $\varepsilon_0 = 1$. The relative permeabilities of all of the spaces are assumed to be μ_0. In other words, space Ω_0 is supposed as free space. $\psi^{\rm s}$ denotes the scattered field in the space Ω_0. In this study, the time dependence is set to be $\mathrm{e}^{-\mathrm{i}\,\omega t}$ and the position vector is $\boldsymbol{r} = x\hat{\boldsymbol{x}} + z\hat{\boldsymbol{z}}$.

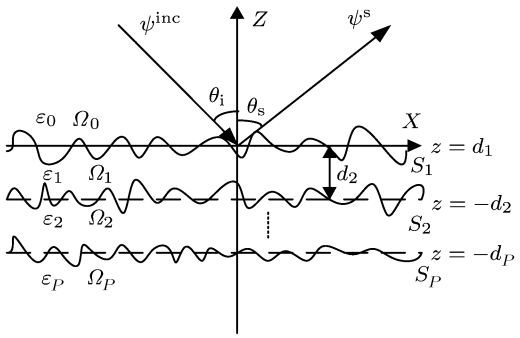


Fig. 1. Geometric model of EM scattering from p-layered rough surfaces without an object.

In this study, to avoid artificial edge diffraction resulting from the finite length of the simulated rough surfaces, the tapered wave suggested by Thorsos, in which the energy is distributed in a narrow beam for the mean incident angle, is chosen as the incident wave that illuminates the geometry model (as shown in Fig. 1) and can be written as[17]

$$\begin{aligned}\boldsymbol{\psi}^{\rm inc}(\boldsymbol{r}) &= \hat{\boldsymbol{y}}\psi^{\rm inc}(\boldsymbol{r})\\ &= \hat{\boldsymbol{y}}\exp\left[\mathrm{i}\,k_0(x\sin\theta_{\rm i} - z\cos\theta_{\rm i})[1 + w(\boldsymbol{r})]\right]\\ &\quad\times\exp\left(-\frac{(x + z\tan\theta_{\rm i})^2}{g^2}\right),\end{aligned}\tag{1}$$

where g is the tapering parameter with the dimension of length and controls the tapering of the incident wave. The additional factor in phase is

$$w(\boldsymbol{r}) = [2(x + z\tan\theta_{\rm i})^2/g^2 - 1]/(k_0 g\cos\theta_{\rm i})^2.$$

2.1. EM scattering from multi-layered rough surfaces

An incident VV polarized tapered wave $\psi^{\rm inc}(\boldsymbol{r})$ encounters a geometric model as shown in Fig. 1, where the parameters of the pth Gaussian rough surfaces are δ_p and l_p. We define the total fields in the spaces Ω_p $(p = 0, 1, \ldots, P)$ as ψ_p and their normal derivatives as $\partial\psi_p/\partial n_p$ or $\partial\psi_p/\partial n_{p+1}$. In any space Ω_p, the total field $\psi_p(\boldsymbol{r})$ obeys the equation

$$(\boldsymbol{\nabla}^2 + k_p^2)\psi_p(\boldsymbol{r}) = 0,\tag{2}$$

and $k_p = \omega\sqrt{\mu_0\varepsilon_p}$ is the wave-number in space Ω_p. The two-dimensional Green's function obeys the equation

$$(\boldsymbol{\nabla}^2 + k_p^2)G_p(\boldsymbol{r}, \boldsymbol{r}') = -\Lambda(\boldsymbol{r} - \boldsymbol{r}'),\tag{3}$$

where $\Lambda(\boldsymbol{r} - \boldsymbol{r}')$is the Dirac function, and

$$G_p(\boldsymbol{r}, \boldsymbol{r}') = \frac{\mathrm{i}}{4}H_0^{(1)}(k_p|\boldsymbol{r} - \boldsymbol{r}'|).\tag{4}$$

Using the Green's theorem, we have

$$\begin{aligned}&\iint_{\Omega_p} \mathrm{d}\tau[\psi_p(\boldsymbol{r}')\boldsymbol{\nabla}^2 G_p(\boldsymbol{r},\boldsymbol{r}') - G_p(\boldsymbol{r},\boldsymbol{r}')\boldsymbol{\nabla}^2\psi_p(\boldsymbol{r}')]\\ =&\int_{S_p}\mathrm{d}S\left[\psi_p(\boldsymbol{r}')\frac{\partial G_p(\boldsymbol{r},\boldsymbol{r}')}{\partial n_p} - G_p(\boldsymbol{r},\boldsymbol{r}')\frac{\partial\psi_p(\boldsymbol{r}')}{\partial n_p}\right]\\ &-\int_{S_{p+1}}\mathrm{d}S\left[\psi_p(\boldsymbol{r}')\frac{\partial G_p(\boldsymbol{r},\boldsymbol{r}')}{\partial n_{p+1}} - G_p(\boldsymbol{r},\boldsymbol{r}')\frac{\partial\psi_p(\boldsymbol{r}')}{\partial n_{p+1}}\right],\end{aligned} \tag{5}$$

where S_p and S_{p+1} indicate the interfaces of the pth and $(p+1)$th rough surfaces respectively. For $p=0$, surface S_p can be regarded as S_∞, and

$$\begin{aligned}&\int_{S_p}\mathrm{d}S\left[\psi_p(\boldsymbol{r}')\frac{\partial G_p(\boldsymbol{r},\boldsymbol{r}')}{\partial n_p} - G_p(\boldsymbol{r},\boldsymbol{r}')\frac{\partial\psi_p(\boldsymbol{r}')}{\partial n_p}\right]\\ &=-\psi^{\mathrm{inc}}(\boldsymbol{r}),\quad \boldsymbol{r}\in\Omega_0.\end{aligned} \tag{6}$$

For $p=P$, surface S_{p+1} can be treated as $S_{-\infty}$, and

$$\begin{aligned}&\int_{S_{p+1}}\mathrm{d}S\left[\psi_p(\boldsymbol{r}')\frac{\partial G_p(\boldsymbol{r},\boldsymbol{r}')}{\partial n_{p+1}} - G_p(\boldsymbol{r},\boldsymbol{r}')\frac{\partial\psi_p(\boldsymbol{r}')}{\partial n_{p+1}}\right]\\ &=0,\quad \boldsymbol{r}\in\Omega_P.\end{aligned} \tag{7}$$

Substituting Eqs. (2) and (3) into the left-hand side of Eq. (5), one have

$$\begin{aligned}&\iint_{\Omega_p} \mathrm{d}\tau[\psi_p(\boldsymbol{r}')\boldsymbol{\nabla}^2 G_p(\boldsymbol{r},\boldsymbol{r}') - G_p(\boldsymbol{r},\boldsymbol{r}')\boldsymbol{\nabla}^2\psi_p(\boldsymbol{r}')]\\ &=-\iint_{\Omega_p}\mathrm{d}\tau\psi_p(\boldsymbol{r}')\Lambda(\boldsymbol{r}-\boldsymbol{r}')\\ &=\begin{cases}-\psi_p(\boldsymbol{r}), & \boldsymbol{r}\in\Omega_p,\\ 0, & \text{else.}\end{cases}\end{aligned} \tag{8}$$

Then, in space Ω_p, the total field ψ_p and its normal derivatives $\partial\psi_p/\partial n_p$ or $\partial\psi_p/\partial n_{p+1}$ satisfy the following integral equation:

$$\begin{aligned}&-\psi_p(\boldsymbol{r})\\ &=\int_{S_p}\mathrm{d}S\left[\psi_p(\boldsymbol{r}')\frac{\partial G_p(\boldsymbol{r},\boldsymbol{r}')}{\partial n_p} - G_p(\boldsymbol{r},\boldsymbol{r}')\frac{\partial\psi_p(\boldsymbol{r}')}{\partial n_p}\right]\\ &\quad-\int_{S_{p+1}}\mathrm{d}S\left[\psi_p(\boldsymbol{r}')\frac{\partial G_p(\boldsymbol{r},\boldsymbol{r}')}{\partial n_{p+1}} - G_p(\boldsymbol{r},\boldsymbol{r}')\frac{\partial\psi_p(\boldsymbol{r}')}{\partial n_{p+1}}\right],\\ &\quad\boldsymbol{r}\in\Omega_p.\end{aligned} \tag{9}$$

For $\boldsymbol{r}\in\Omega_p$ and $\boldsymbol{r}\in S_p$, the first term of the right-hand side is

$$\begin{aligned}&\int_{S_p}\mathrm{d}S\left[\psi_p(\boldsymbol{r}')\frac{\partial G_p(\boldsymbol{r},\boldsymbol{r}')}{\partial n_p}\right]\\ &=-\frac{1}{2}\psi_p(\boldsymbol{r})+\int_{S_p\mathrm{P.V.}}\mathrm{d}S\left[\psi_p(\boldsymbol{r}')\frac{\partial G_p(\boldsymbol{r},\boldsymbol{r}')}{\partial n_p}\right],\end{aligned} \tag{10}$$

where P.V. refers to the Cauchy principal value integral on the interface S_p. For $\boldsymbol{r}\in\Omega_p$ and $\boldsymbol{r}\in S_{p+1}$, the second term of the right-hand side is

$$\begin{aligned}&-\int_{S_{p+1}}\mathrm{d}S\left[\psi_p(\boldsymbol{r}')\frac{\partial G_p(\boldsymbol{r},\boldsymbol{r}')}{\partial n_{p+1}}\right]\\ &=-\frac{1}{2}\psi_p(\boldsymbol{r})-\int_{S_{p+1\mathrm{P.V.}}}\mathrm{d}S\left[\psi_p(\boldsymbol{r}')\frac{\partial G_p(\boldsymbol{r},\boldsymbol{r}')}{\partial n_{p+1}}\right],\end{aligned} \tag{11}$$

and P.V. indicates the Cauchy principal value integral on the interface S_{p+1}. Using Eqs. (9) and (10), one have

$$\begin{aligned}0=&\frac{1}{2}\psi_p(\boldsymbol{r})+\int_{S_p\mathrm{P.V.}}\mathrm{d}S\left[\psi_p(\boldsymbol{r}')\frac{\partial G_p(\boldsymbol{r},\boldsymbol{r}')}{\partial n_p}\right]\\ &-\int_{S_p}\mathrm{d}S\left[G_p(\boldsymbol{r},\boldsymbol{r}')\frac{\partial\psi_p(\boldsymbol{r}')}{\partial n_p}\right]\\ &-\int_{S_{p+1}}\mathrm{d}S\Bigg[\psi_p(\boldsymbol{r}')\frac{\partial G_p(\boldsymbol{r},\boldsymbol{r}')}{\partial n_{p+1}}\\ &-G_p(\boldsymbol{r},\boldsymbol{r}')\frac{\partial\psi_p(\boldsymbol{r}')}{\partial n_{p+1}}\Bigg],\quad \boldsymbol{r}\in\Omega_p,\ \boldsymbol{r}\in S_p.\end{aligned} \tag{12}$$

Similarly, using Eqs. (9) and (11), one obtain

$$\begin{aligned}0=&\frac{1}{2}\psi_p(\boldsymbol{r})\\ &+\int_{S_p}\mathrm{d}S\left[\psi_p(\boldsymbol{r}')\frac{\partial G_p(\boldsymbol{r},\boldsymbol{r}')}{\partial n_p} - G_p(\boldsymbol{r},\boldsymbol{r}')\frac{\partial\psi_p(\boldsymbol{r}')}{\partial n_p}\right]\\ &-\int_{S_{p+1}\mathrm{P.V.}}\mathrm{d}S\left[\psi_p(\boldsymbol{r}')\frac{\partial G_p(\boldsymbol{r},\boldsymbol{r}')}{\partial n_{p+1}}\right]\\ &+\int_{S_{p+1}}\mathrm{d}S\left[G_p(\boldsymbol{r},\boldsymbol{r}')\frac{\partial\psi_p(\boldsymbol{r}')}{\partial n_{p+1}}\right],\\ &\boldsymbol{r}\in\Omega_p,\ \boldsymbol{r}\in S_{p+1}.\end{aligned} \tag{13}$$

It is necessary to note that the total fields and their normal derivatives on the pth rough surfaces are our focus. That is to say, for $p=0$, only Eq. (13) is considerable, and for $p=P$, only Eq. (12) is sufficient.

When point $\boldsymbol{r}$ is put on the interface of the pth $(p=1,2,\ldots,P)$ rough surface, the total field ψ_p and its normal derivative $\partial\psi_p/\partial n_p$ satisfy the following boundary conditions:

$$\psi_{p-1}(\boldsymbol{r})=\psi_p(\boldsymbol{r}),\quad \frac{\partial\psi_{p-1}(\boldsymbol{r})}{\partial n_p}=\frac{1}{\rho_{pp-1}}\frac{\partial\psi_p(\boldsymbol{r})}{\partial n_p}, \tag{14}$$

for the horizontal polarization, $\rho_{pp-1}=1$, and for VV polarization, $\rho_{pp-1}=\varepsilon_p/\varepsilon_{p-1}$.

Hence, one can obtain the matrix equation of the surface unknowns $I_{2\times p-1}(\boldsymbol{r})=\psi_{p-1}(\boldsymbol{r})(\boldsymbol{r}\in S_p)$ and

$$I_{2\times p}(\boldsymbol{r})=\frac{\partial\psi_{p-1}(\boldsymbol{r})}{\partial n_p},\quad (\boldsymbol{r}\in S_p)$$

as

$$\begin{bmatrix}\bar{\bar{\boldsymbol{A}}}^{(p-1)} & \bar{\bar{\boldsymbol{B}}}^{(p-1)}\\ \bar{\bar{\boldsymbol{C}}}^{p} & -\rho_{pp-1}\bar{\bar{\boldsymbol{D}}}^{p}\end{bmatrix}\begin{bmatrix}\bar{\boldsymbol{I}}_{2\times p-1}\\ \bar{\boldsymbol{I}}_{2\times p}\end{bmatrix}=\begin{bmatrix}\bar{\boldsymbol{V}}_{2\times p-1}\\ \bar{\boldsymbol{V}}_{2\times p}\end{bmatrix}, \tag{15}$$

where $\bar{\boldsymbol{V}}_1(\boldsymbol{r}) = \bar{\psi}^{\rm inc}(\boldsymbol{r})$, $\bar{\boldsymbol{V}}_q(\boldsymbol{r}) = \bar{\boldsymbol{0}}(q = 2, 3, \ldots, 2\times P)$. Elements of $\bar{\bar{\boldsymbol{A}}}^{(p-1)}$, $\bar{\bar{\boldsymbol{B}}}^{(p-1)}$, $\bar{\bar{\boldsymbol{C}}}^{p}$, $\bar{\bar{D}}^{p}$ are

$$A_{mn}^{(p-1)} = \begin{cases} -\Delta l_n^p \dfrac{\mathrm{i}\,k_{p-1}}{4}(\hat{\boldsymbol{n}}_p \cdot \boldsymbol{R}_p) H_1^{(1)}(k_{p-1}\,|\boldsymbol{r}_m - \boldsymbol{r}_n|), & m \neq n, \\ \dfrac{1}{2} - \dfrac{f_p''(x_m)\Delta x}{4\pi[1 + f_p'^2(x_m)]}, & m = n, \end{cases} \tag{16}$$

$$B_{mn}^{(p-1)} = \begin{cases} \Delta l_n^p \dfrac{\mathrm{i}}{4} H_0^{(1)}(k_{p-1}\,|\boldsymbol{r}_m - \boldsymbol{r}_n|), & m \neq n, \\ \Delta l_m^p \dfrac{\mathrm{i}}{4} H_0^{(1)}[k_{p-1}\Delta l_m^p/(2e)], & m = n, \end{cases} \tag{17}$$

$$C_{mn}^{p} = \begin{cases} \Delta l_n^p \dfrac{\mathrm{i}\,k_p}{4}(\hat{\boldsymbol{n}}_p \cdot \boldsymbol{R}_p) H_1^{(1)}(k_p\,|\boldsymbol{r}_m - \boldsymbol{r}_n|), & m \neq n, \\ \dfrac{1}{2} + \dfrac{f''_p(x_m)\Delta x}{4\pi[1 + f_p'^2(x_m)]}, & m = n, \end{cases} \tag{18}$$

$$D_{mn}^{p} = \begin{cases} \Delta l_n^p \dfrac{\mathrm{i}}{4} H_0^{(1)}(k_p\,|\boldsymbol{r}_m - \boldsymbol{r}_n|), & m \neq n, \\ \Delta l_m^p \dfrac{\mathrm{i}}{4} H_0^{(1)}[k_p\Delta l_m^p/(2e)], & m = n, \end{cases} \tag{19}$$

where $\boldsymbol{r}_m, \boldsymbol{r}_n$ are the field point and source point on the pth rough surface, respectively, $f'_p(x)$ and $f''_p(x)$ are the first- and second-order differentials of $f_p(x)$, $e = 2.7182138$, and

$$\begin{aligned} \Delta l_n^p &= \Delta x\sqrt{1 + [f'_p(x_n)]^2}, \\ \Delta l_m^p &= \Delta x\sqrt{1 + [f'_p(x_m)]^2}, \\ \hat{\boldsymbol{n}}_p &= \frac{-f'_p(x_n)\hat{\boldsymbol{x}} + \hat{\boldsymbol{z}}}{\sqrt{1 + [f'_p(x_n)]^2}}, \end{aligned} \tag{20}$$

$$\boldsymbol{R}_p = \frac{\boldsymbol{r}_m - \boldsymbol{r}_n}{|\boldsymbol{r}_m - \boldsymbol{r}_n|}. \tag{21}$$

It is necessary to point out that the four matrixes $\bar{\bar{\boldsymbol{A}}}^{(p-1)}$, $\bar{\bar{\boldsymbol{B}}}^{(p-1)}$, $\bar{\bar{\boldsymbol{C}}}^{p}$, $\bar{\bar{\boldsymbol{D}}}^{p}$ are only associated with the pth rough surface. Interactions between the pth rough surface and the $(p+1)$th rough surface should be considered, then the matrix equation (15) will be changed into

$$\begin{bmatrix} \bar{\bar{\boldsymbol{A}}}^{(p-1)} & \bar{\bar{\boldsymbol{B}}}^{(p-1)} & \bar{\bar{\boldsymbol{0}}} & \bar{\bar{\boldsymbol{0}}} \\ \bar{\bar{\boldsymbol{C}}}^{p} & -\rho_{pp-1}\bar{\bar{\boldsymbol{D}}}^{p} & \bar{\bar{\boldsymbol{E}}}^{p} & \bar{\bar{\boldsymbol{F}}}^{p} \\ \bar{\bar{\boldsymbol{G}}}^{p} & -\rho_{pp-1}\bar{\bar{\boldsymbol{H}}}^{p} & \bar{\bar{\boldsymbol{A}}}^{p} & \bar{\bar{\boldsymbol{B}}}^{p} \\ \bar{\bar{\boldsymbol{0}}} & \bar{\bar{\boldsymbol{0}}} & \bar{\bar{\boldsymbol{C}}}^{p+1} & -\rho_{p+1p}\bar{\bar{\boldsymbol{D}}}^{p+1} \end{bmatrix} \begin{bmatrix} \bar{\boldsymbol{I}}_{2\times p-1} \\ \bar{\boldsymbol{I}}_{2\times p} \\ \bar{\boldsymbol{I}}_{2\times p+1} \\ \bar{\boldsymbol{I}}_{2\times p+2} \end{bmatrix} = \begin{bmatrix} \bar{\boldsymbol{V}}_{2\times p-1} \\ \bar{\boldsymbol{V}}_{2\times p} \\ \bar{\boldsymbol{V}}_{2\times p+1} \\ \bar{\boldsymbol{V}}_{2\times p+2} \end{bmatrix}, \tag{22}$$

where the elements $\bar{\bar{\boldsymbol{E}}}^{p}$, $\bar{\bar{\boldsymbol{F}}}^{p}$, $\bar{\bar{G}}^{p}$, $\bar{\bar{\boldsymbol{H}}}^{p}$ are

$$E_{mq}^{p} = -\Delta l_q^p \frac{\mathrm{i}\,k_p}{4}(\hat{\boldsymbol{n}}_{p+1} \cdot \boldsymbol{R}_{mq}) H_1^{(1)}(k_p\,|\boldsymbol{r}_m - \boldsymbol{r}_q|), \tag{23}$$

$$F_{mq}^{p} = \Delta l_q^p \frac{\mathrm{i}}{4} H_0^{(1)}(k_p\,|\boldsymbol{r}_m - \boldsymbol{r}_q|), \tag{24}$$

$$G_{pn}^{p} = \Delta l_n^p \frac{\mathrm{i}\,k_p}{4}(\hat{\boldsymbol{n}}_p \cdot \boldsymbol{R}_{pn}) H_1^{(1)}(k_p\,|\boldsymbol{r}_p - \boldsymbol{r}_n|), \tag{25}$$

$$H_{pn}^{p} = \Delta l_n^p \frac{\mathrm{i}}{4} H_0^{(1)}(k_p\,|\boldsymbol{r}_p - \boldsymbol{r}_n|). \tag{26}$$

Here, $\boldsymbol{r}_p$, $\boldsymbol{r}_q$ are the field point and source point on the $(p+1)$th rough surface, and

$$\boldsymbol{R}_{mq} = \frac{\boldsymbol{r}_m - \boldsymbol{r}_q}{|\boldsymbol{r}_m - \boldsymbol{r}_q|}, \quad \boldsymbol{R}_{pn} = \frac{\boldsymbol{r}_p - \boldsymbol{r}_n}{|\boldsymbol{r}_p - \boldsymbol{r}_n|}. \tag{27}$$

Therefore, one can obtain the matrix equation of EM scattering from a two-layered rough surface[8]

$$\begin{bmatrix} \bar{\bar{\boldsymbol{A}}}^{0} & \bar{\bar{\boldsymbol{B}}}^{0} & \bar{\bar{\boldsymbol{0}}} & \bar{\bar{\boldsymbol{0}}} \\ \bar{\bar{\boldsymbol{C}}}^{1} & -\rho_{10}\bar{\bar{\boldsymbol{D}}}^{1} & \bar{\bar{\boldsymbol{E}}}^{1} & \bar{\bar{\boldsymbol{F}}}^{1} \\ \bar{\bar{\boldsymbol{G}}}^{1} & -\rho_{10}\bar{\bar{\boldsymbol{H}}}^{1} & \bar{\bar{\boldsymbol{A}}}^{1} & \bar{\bar{\boldsymbol{B}}}^{1} \\ \bar{\bar{\boldsymbol{0}}} & \bar{\bar{\boldsymbol{0}}} & \bar{\bar{\boldsymbol{C}}}^{2} & -\rho_{21}\bar{\bar{\boldsymbol{D}}}^{2} \end{bmatrix} \begin{bmatrix} \bar{\boldsymbol{I}}_1 \\ \bar{\boldsymbol{I}}_2 \\ \bar{\boldsymbol{I}}_3 \\ \bar{\boldsymbol{I}}_4 \end{bmatrix} = \begin{bmatrix} \bar{\psi}^{\rm inc} \\ \bar{\bar{\boldsymbol{0}}} \\ \bar{\bar{\boldsymbol{0}}} \\ \bar{\bar{\boldsymbol{0}}} \end{bmatrix}. \tag{28}$$

After solving the matrix equation through the BICGM, the surface unknowns $\bar{\boldsymbol{I}}_1 \sim \bar{\boldsymbol{I}}_{2\times P}$ can be obtained. When the point $\boldsymbol{R}$ is located in the far field, and for observation in the $\boldsymbol{k}_{\rm s} = k_0(\hat{\boldsymbol{x}}\sin\theta_{\rm s} + \hat{\boldsymbol{z}}\cos\theta_{\rm s})$ direction, the scattered field $\psi^{\rm s}$ in the space Ω_0 is[15]

$$\psi^{\rm s}(\boldsymbol{R}) = \frac{\mathrm{i}}{4}\sqrt{\frac{2}{\pi k_0 R}}\exp\left(\mathrm{i}\,k_0 R - \mathrm{i}\,\frac{\pi}{4}\right)\psi_{\rm s}^{N}(\theta_{\rm s}, \theta_{\rm i}), \tag{29}$$

where

$$\begin{aligned} \psi_{\rm s}^{N}(\theta_{\rm s}, \theta_{\rm i}) = &\int_{S_1} [-\mathrm{i}(\hat{\boldsymbol{n}}_1 \cdot \boldsymbol{k}_{\rm s}) I_1(x) - I_2(x)] \\ &\times \exp(-\mathrm{i}\,\boldsymbol{k}_{\rm s} \cdot \boldsymbol{R}_1)\sqrt{1 + [f'_1(x)]^2}\mathrm{d}x, \end{aligned} \tag{30}$$

and $\boldsymbol{R}_1 = \hat{\boldsymbol{x}}x + \hat{\boldsymbol{z}}f_1(x)$. Then the BSC can also be defined as[15]

$$\sigma(\theta_{\rm s}) = \frac{\left|\psi_{\rm s}^N(\theta_{\rm s},\theta_{\rm i})\right|^2}{8\pi k_0 g\sqrt{\frac{\pi}{2}}\cos\theta_{\rm i}\left(1-\frac{1+2\tan^2\theta_{\rm i}}{2k_0^2g^2\cos^2\theta_{\rm i}}\right)}. \quad (31)$$

2.2. EM scattering from a PEC object and multi-layered rough surfaces

If a PEC object is located in the space Ω_p (see Fig. 2), between the pth rough surface and the $(p+1)$th rough surface, there will be induced current on the object too. For the VV polarized wave, the total field $\psi_p(\boldsymbol{r})$ obeys

$$\frac{\partial\psi_p(\boldsymbol{r})}{\partial n_{\rm o}} = 0, \quad \boldsymbol{r}\in S_{\rm o},$$

where $S_{\rm o}$ and $\hat{\boldsymbol{n}}_{\rm o}$ represent the interface and normal vector of the object. Then the integral equation (9) is transformed into

$$\begin{aligned}-\psi_p(\boldsymbol{r}) = &\int_{S_{\rm o}} {\rm d}S\left[\psi_p(\boldsymbol{r}')\frac{\partial G_p(\boldsymbol{r},\boldsymbol{r}')}{\partial n_p}\right]\\ &+\int_{S_p}{\rm d}S\Big[\psi_p(\boldsymbol{r}')\frac{\partial G_p(\boldsymbol{r},\boldsymbol{r}')}{\partial n_p}\\ &-G_p(\boldsymbol{r},\boldsymbol{r}')\frac{\partial\psi_p(\boldsymbol{r}')}{\partial n_p}\Big]\\ &-\int_{S_{p+1}}{\rm d}S\Big[\psi_p(\boldsymbol{r}')\frac{\partial G_p(\boldsymbol{r},\boldsymbol{r}')}{\partial n_{p+1}}\\ &-G_p(\boldsymbol{r},\boldsymbol{r}')\frac{\partial\psi_p(\boldsymbol{r}')}{\partial n_{p+1}}\Big], \quad \boldsymbol{r}\in\Omega_p. \quad (32)\end{aligned}$$

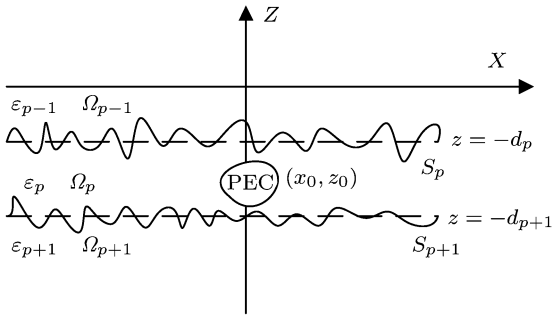


Fig. 2. A PEC object located in Ω_p between the pth and the $(p+1)$th rough surfaces.

Here, contributions of $\psi_p(\boldsymbol{r})(\boldsymbol{r}\in S_{\rm o})$ are considered. Matrix equation (22) is rewritten as

$$\begin{bmatrix} \bar{\bar{\boldsymbol{A}}}^{(p-1)} & \bar{\bar{\boldsymbol{B}}}^{(p-1)} & \bar{\bar{\boldsymbol{0}}} & \bar{\bar{\boldsymbol{0}}} & \bar{\bar{\boldsymbol{0}}} \\ \bar{\bar{\boldsymbol{C}}}^{p} & -\rho_{pp-1}\bar{\bar{\boldsymbol{D}}}^{p} & \bar{\bar{\boldsymbol{E}}}^{p} & \bar{\bar{\boldsymbol{F}}}^{p} & \bar{\bar{\boldsymbol{B}}}^{\rm o} \\ \bar{\bar{\boldsymbol{G}}}^{p} & -\rho_{pp-1}\bar{\bar{\boldsymbol{H}}}^{p} & \bar{\bar{\boldsymbol{A}}}^{p} & \bar{\bar{\boldsymbol{B}}}^{p} & \bar{\bar{\boldsymbol{C}}}^{\rm o} \\ \bar{\bar{\boldsymbol{0}}} & \bar{\bar{\boldsymbol{0}}} & \bar{\bar{\boldsymbol{C}}}^{p+1} & -\rho_{p+1p}\bar{\bar{\boldsymbol{D}}}^{p+1} & \bar{\bar{\boldsymbol{0}}} \\ \bar{\bar{\boldsymbol{E}}}^{\rm o} & \bar{\bar{\boldsymbol{F}}}^{\rm o} & \bar{\bar{G}}^{\rm o} & \bar{\bar{\boldsymbol{H}}}^{\rm o} & \bar{\bar{\boldsymbol{A}}}^{\rm o} \end{bmatrix} \begin{bmatrix} \bar{\boldsymbol{I}}_{2*p-1} \\ \bar{\boldsymbol{I}}_{2*p} \\ \bar{\boldsymbol{I}}_{2*p+1} \\ \bar{\boldsymbol{I}}_{2*p+2} \\ \bar{\boldsymbol{I}}^{\rm o} \end{bmatrix} = \begin{bmatrix} \bar{\boldsymbol{V}}_{2*p-1} \\ \bar{\boldsymbol{V}}_{2*p} \\ \bar{\boldsymbol{V}}_{2*p+1} \\ \bar{\boldsymbol{V}}_{2*p+2} \\ \bar{\boldsymbol{V}}^{\rm o} \end{bmatrix}, \quad (33)$$

where $I^{\rm o}(\boldsymbol{r}) = \psi_{p-1}(\boldsymbol{r})(\boldsymbol{r}\in S_{\rm o})$, $\bar{\boldsymbol{V}}^{\rm o}(\boldsymbol{r}) = \bar{\boldsymbol{\psi}}^{\rm inc}(\boldsymbol{r})(p=0)$, $\bar{\boldsymbol{V}}^{\rm o}(\boldsymbol{r}) = \bar{\boldsymbol{0}}$ $(p=1,2,\ldots,P)$, and

$$A_{st}^{\rm o} = \begin{cases} -\Delta_t\dfrac{{\rm i}\,k_p}{4}(\hat{\boldsymbol{n}}_{\rm o}\cdot\boldsymbol{R}_{\rm o})H_1^{(1)}(k_p\left|\boldsymbol{r}_{\rm s}-\boldsymbol{r}_t\right|), & s\neq t, \\ \dfrac{1}{2}-\dfrac{Z_{\rm o}''(x_t)\Delta x_{\rm o}}{4\pi[1+Z_{\rm o}'^2(x_t)]}, & s=t, \end{cases} \quad (34)$$

$$B_{mt}^{\rm o} = -\Delta l_t\frac{{\rm i}\,k_p}{4}(\hat{\boldsymbol{n}}_{\rm o}\cdot\boldsymbol{R}_{mt})H_1^{(1)}(k_p\left|\boldsymbol{r}_m-\boldsymbol{r}_t\right|), \quad (35)$$

$$E_{sn}^{\rm o} = \Delta l_n\frac{{\rm i}\,k_p}{4}(\hat{\boldsymbol{n}}_p\cdot\boldsymbol{R}_{sn})H_1^{(1)}(k_p\left|\boldsymbol{r}_{\rm s}-\boldsymbol{r}_n\right|), \quad (36)$$

$$F_{sn}^{\rm o} = \Delta l_n\frac{\rm i}{4}H_0^{(1)}(k_p\left|\boldsymbol{r}_{\rm s}-\boldsymbol{r}_n\right|), \quad (37)$$

$$C_{pt}^{\rm o} = -\Delta l_t\frac{{\rm i}\,k_p}{4}(\hat{\boldsymbol{n}}_{\rm o}\cdot\boldsymbol{R}_{pt})H_1^{(1)}(k_p\left|\boldsymbol{r}_p-\boldsymbol{r}_t\right|), \quad (38)$$

$$G_{sq}^{\rm o} = -\Delta l_q\frac{{\rm i}\,k_p}{4}(\hat{n}_{p+1}\cdot\boldsymbol{R}_{sq})H_1^{(1)}(k_p\left|\boldsymbol{r}_{\rm s}-\boldsymbol{r}_q\right|), \quad (39)$$

$$H_{sq}^{\rm o} = \Delta l_q\frac{\rm i}{4}H_0^{(1)}(k_p\left|\boldsymbol{r}_{\rm s}-\boldsymbol{r}_q\right|), \quad (40)$$

where, $\boldsymbol{r}_{\rm s},\boldsymbol{r}_t$ are the field point and source point on the object, $Z_{\rm o}(x)$ is the height profile of the object, $Z_{\rm o}'(x)$ and $Z_{\rm o}''(x)$ are the first- and second-order differentials of $Z_{\rm o}(x)$, $\Delta x_{\rm o}$ is the interval of the object interface, and

$$\begin{aligned}\Delta l_t &= \Delta x_{\rm o}\sqrt{1+[Z_{\rm o}'(x_t)]^2},\\ \hat{\boldsymbol{n}}_{\rm o} &= \frac{-Z_{\rm o}'(x_t)\hat{\boldsymbol{x}}+\hat{z}}{\sqrt{1+[Z_{\rm o}'(x_t)]^2}},\\ \boldsymbol{R}_{\rm o} &= \frac{\boldsymbol{r}_{\rm s}-\boldsymbol{r}_t}{|\boldsymbol{r}_{\rm s}-\boldsymbol{r}_t|}, \quad \boldsymbol{R}_{mt} = \frac{\boldsymbol{r}_m-\boldsymbol{r}_t}{|\boldsymbol{r}_m-\boldsymbol{r}_t|},\end{aligned} \quad (41)$$

$$\boldsymbol{R}_{sn} = \frac{\boldsymbol{r}_{\rm s} - \boldsymbol{r}_n}{|\boldsymbol{r}_{\rm s} - \boldsymbol{r}_n|}, \quad \boldsymbol{R}_{pt} = \frac{\boldsymbol{r}_p - \boldsymbol{r}_t}{|\boldsymbol{r}_p - \boldsymbol{r}_t|},$$
$$\boldsymbol{R}_{sq} = \frac{\boldsymbol{r}_{\rm s} - \boldsymbol{r}_q}{|\boldsymbol{r}_{\rm s} - \boldsymbol{r}_q|}. \tag{42}$$

The matrix $\bar{\bar{\boldsymbol{A}}}^{\rm o}$ depends only on the object. Matrixes $\bar{\bar{\boldsymbol{B}}}^{\rm o}$, $\bar{\bar{\boldsymbol{E}}}^{\rm o}$, $\bar{\bar{\boldsymbol{F}}}^{\rm o}$ show the interactions between the object and the pth rough surface. Matrixes $\bar{\bar{\boldsymbol{C}}}^{\rm o}$, $\bar{\bar{\boldsymbol{G}}}^{\rm o}$, $\bar{\bar{\boldsymbol{H}}}^{\rm o}$ represent the relationship of the object and the $(p+1)$th rough surface.

Therefore, for case A: $p = 0$, a PEC object is located above a two-layered rough surface, the matrix equation is[19]

$$\begin{bmatrix} \bar{\bar{\boldsymbol{A}}}^0 & \bar{\bar{\boldsymbol{B}}}^0 & \bar{\bar{\boldsymbol{0}}} & \bar{\bar{\boldsymbol{0}}} & \bar{\bar{\boldsymbol{C}}}^{\rm o} \\ \bar{\bar{\boldsymbol{C}}}^1 & -\rho_{10}\bar{\bar{\boldsymbol{D}}}^1 & \bar{\bar{\boldsymbol{E}}}^1 & \bar{\bar{\boldsymbol{F}}}^1 & \bar{\bar{\boldsymbol{0}}} \\ \bar{\bar{\boldsymbol{G}}}^1 & -\rho_{10}\bar{\bar{\boldsymbol{H}}}^1 & \bar{\bar{\boldsymbol{A}}}^1 & \bar{\bar{\boldsymbol{B}}}^1 & \bar{\bar{\boldsymbol{0}}} \\ \bar{\bar{\boldsymbol{0}}} & \bar{\bar{\boldsymbol{0}}} & \bar{\bar{\boldsymbol{C}}}^2 & -\rho_{21}\bar{\bar{\boldsymbol{D}}}^2 & \bar{\bar{\boldsymbol{0}}} \\ \bar{\bar{\boldsymbol{G}}}^{\rm o} & \bar{\bar{\boldsymbol{H}}}^{\rm o} & \bar{\bar{\boldsymbol{0}}} & \bar{\bar{\boldsymbol{0}}} & \bar{\bar{\boldsymbol{A}}}^{\rm o} \end{bmatrix} \begin{bmatrix} \bar{\boldsymbol{I}}_1 \\ \bar{\boldsymbol{I}}_2 \\ \bar{\boldsymbol{I}}_3 \\ \bar{\boldsymbol{I}}_4 \\ \bar{\boldsymbol{I}}^{\rm o} \end{bmatrix} = \begin{bmatrix} \bar{\psi}^{\rm inc} \\ \bar{\bar{\boldsymbol{0}}} \\ \bar{\bar{\boldsymbol{0}}} \\ \bar{\bar{\boldsymbol{0}}} \\ \bar{\psi}^{\rm inc} \end{bmatrix}. \tag{43}$$

For case B: $p = 1$, the PEC object is located between the two-layered rough surface, the matrix equation is

$$\begin{bmatrix} \bar{\bar{\boldsymbol{A}}}^0 & \bar{\bar{\boldsymbol{B}}}^0 & \bar{\bar{\boldsymbol{0}}} & \bar{\bar{\boldsymbol{0}}} & \bar{\bar{\boldsymbol{0}}} \\ \bar{\bar{\boldsymbol{C}}}^1 & -\rho_{10}\bar{\bar{\boldsymbol{D}}}^1 & \bar{\bar{\boldsymbol{E}}}^1 & \bar{\bar{\boldsymbol{F}}}^1 & \bar{\bar{\boldsymbol{B}}}^{\rm o} \\ \bar{\bar{\boldsymbol{G}}}^1 & -\rho_{10}\bar{\bar{\boldsymbol{H}}}^1 & \bar{\bar{\boldsymbol{A}}}^1 & \bar{\bar{\boldsymbol{B}}}^1 & \bar{\bar{\boldsymbol{C}}}^{\rm o} \\ \bar{\bar{\boldsymbol{0}}} & \bar{\bar{\boldsymbol{0}}} & \bar{\bar{\boldsymbol{C}}}^2 & -\rho_{21}\bar{\bar{\boldsymbol{D}}}^2 & \bar{\bar{\boldsymbol{0}}} \\ \bar{\bar{\boldsymbol{E}}}^{\rm o} & \bar{\bar{\boldsymbol{F}}}^{\rm o} & \bar{\bar{\boldsymbol{G}}}^{\rm o} & \bar{\bar{\boldsymbol{H}}}^{\rm o} & \bar{\bar{\boldsymbol{A}}}^{\rm o} \end{bmatrix} \begin{bmatrix} \bar{\boldsymbol{I}}_1 \\ \bar{\boldsymbol{I}}_2 \\ \bar{\boldsymbol{I}}_3 \\ \bar{\boldsymbol{I}}_4 \\ \bar{\boldsymbol{I}}^{\rm o} \end{bmatrix} = \begin{bmatrix} \bar{\psi}^{\rm inc} \\ \bar{\bar{\boldsymbol{0}}} \\ \bar{\bar{\boldsymbol{0}}} \\ \bar{\bar{\boldsymbol{0}}} \\ \bar{\bar{\boldsymbol{0}}} \end{bmatrix}. \tag{44}$$

For case C: $p = 2$, the PEC object is located below the two-layered rough surface, the matrix equation is[20]

$$\begin{bmatrix} \bar{\bar{\boldsymbol{A}}}^0 & \bar{\bar{\boldsymbol{B}}}^0 & \bar{\bar{\boldsymbol{0}}} & \bar{\bar{\boldsymbol{0}}} & \bar{\bar{\boldsymbol{0}}} \\ \bar{\bar{\boldsymbol{C}}}^1 & -\rho_{10}\bar{\bar{\boldsymbol{D}}}^1 & \bar{\bar{\boldsymbol{E}}}^1 & \bar{\bar{\boldsymbol{F}}}^1 & \bar{\bar{\boldsymbol{0}}} \\ \bar{\bar{\boldsymbol{G}}}^1 & -\rho_{10}\bar{\bar{\boldsymbol{H}}}^1 & \bar{\bar{\boldsymbol{A}}}^1 & \bar{\bar{\boldsymbol{B}}}^1 & \bar{\bar{\boldsymbol{0}}} \\ \bar{\bar{\boldsymbol{0}}} & \bar{\bar{\boldsymbol{0}}} & \bar{\bar{\boldsymbol{C}}}^2 & -\rho_{21}\bar{\bar{\boldsymbol{D}}}^2 & \bar{\bar{\boldsymbol{B}}}^{\rm o} \\ \bar{\bar{\boldsymbol{0}}} & \bar{\bar{\boldsymbol{0}}} & \bar{\bar{\boldsymbol{E}}}^{\rm o} & \bar{\bar{\boldsymbol{F}}}^{\rm o} & \bar{\bar{\boldsymbol{A}}}^{\rm o} \end{bmatrix} \begin{bmatrix} \bar{\boldsymbol{I}}_1 \\ \bar{\boldsymbol{I}}_2 \\ \bar{\boldsymbol{I}}_3 \\ \bar{\boldsymbol{I}}_4 \\ \bar{\boldsymbol{I}}^{\rm o} \end{bmatrix} = \begin{bmatrix} \bar{\psi}^{\rm inc} \\ \bar{\bar{\boldsymbol{0}}} \\ \bar{\bar{\boldsymbol{0}}} \\ \bar{\bar{\boldsymbol{0}}} \\ \bar{\bar{\boldsymbol{0}}} \end{bmatrix}. \tag{45}$$

For case A, contributions of $\psi_0(\boldsymbol{r})(\boldsymbol{r} \in S_{\rm o})$ to the scattered field should not be neglected. Hence, Eq. (30) is changed into

$$\psi_{\rm s}^N(\theta_{\rm s}, \theta_{\rm i}) = \int_{S_1} [-{\rm i}(\hat{\boldsymbol{n}}_1 \cdot \boldsymbol{k}_{\rm s}) I_1(x) - I_2(x)] \times \exp(-{\rm i}\,\boldsymbol{k}_{\rm s} \cdot \boldsymbol{R}_1)\sqrt{1 + [f'_1(x)]^2}{\rm d}x + \int_{S_{\rm o}} [-{\rm i}(\hat{\boldsymbol{n}}_{\rm o} \cdot \boldsymbol{k}_{\rm s}) I^{\rm o}(x)] \times \exp(-{\rm i}\,\boldsymbol{k}_{\rm s} \cdot \boldsymbol{R}_{\rm o})\sqrt{1 + [Z'_{\rm o}(x)]^2}{\rm d}x, \tag{46}$$

and

$$\boldsymbol{R}_{\rm o} = \hat{\boldsymbol{x}}x + \hat{\boldsymbol{z}}Z_{\rm o}(x).$$

Definitions of the scattered field in the space Ω_0 and the BSC are the same as Eqs. (29) and (31).

For cases B and C, definitions of the scattered field and the BSC are only the same as those of a multi-layered rough surface. That is because only $\psi_0(\boldsymbol{r})(\boldsymbol{r} \in S_1)$ and $\partial\psi_0(\boldsymbol{r})/\partial n_1(\boldsymbol{r} \in S_1)$ contribute to the scattered field.

3. Numerical simulations and discussion

Firstly, to ensure the validity of the algorithm presented in this paper, the angular distributions of the BSC in cases A and C were compared with those from existing scattering models, which have been studied in Refs. [6, 18]. In Fig. 3(a), the results marked as single-layered model are obtained through the MOM algorithm proposed by Wang *et al.* in Ref. [18]. For cases A and C in this paper, $\varepsilon_1 = \varepsilon_2$, the two-layered rough surface model can be regarded as the single-layered model. The cylinder was located at $x_p = 0$, $z_p = 5\lambda$ (case A) or $x_p = 0$, $z_p = -10\lambda$ (case C) with radius $r = \lambda$. The parameters of the Gaussian rough surface were set to be $\delta = 0.2\lambda$, $l = \lambda$. From Fig. 3(a), it can be clearly seen that the angular distributions of the BSC in this work are in good agreement with those of the existing solution in Ref. [18]. In Fig. 3(b), the radius of the cylinder was assumed to be small enough ($r = 1.0 \times 10^{-6}\lambda$) for the contributions of the cylinder to the BSC to be neglected. The scattering pattern labelled as without object is computed by the MOM algorithm and has been studied using the PILE method in Ref. [6]. The parameters of the two Gaussian rough surfaces were $\delta_1 = 0.2\lambda$, $l_1 = \lambda$, $d_1 = 0$ and $\delta_2 = 0.3\lambda$, $l_2 = 1.5\lambda$, $d_2 = 5\lambda$. It is clear that the scattering patterns of the three scattering models are almost the same over the whole scattering region. Consequently, the results of Fig. 3 demonstrate the effectiveness and accuracy of the MOM algorithm presented in this paper.

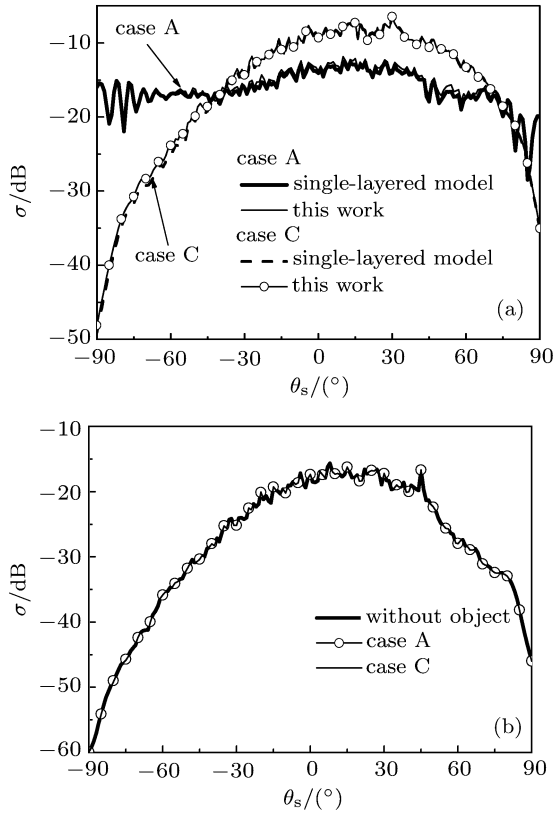


Fig. 3. Comparison of BSC of this work with that of existing scattering models (a) with the model of Ref. [18], and (b) with the model of Ref. [6].

In the following numerical simulations, the two Gaussian rough surfaces are divided into $N = 1024$ segments with $\Delta x = \lambda/10$, which indicate that the simulated lengths were $L = 102.4\lambda$. The cylinder was located at $x_p = 0$ with segments $N_0 = 100$. The parameters of the tapered wave were set to be $\lambda = 0.3$ m, $\theta_i = 30°$, $g = L/4$. The two Gaussian rough surfaces were $\delta_1 = 0.2\lambda$, $l_1 = 1.0\lambda$, $\delta_2 = 0.5\lambda$, $l_2 = 1.5\lambda$ except in Fig. 6. All numerical simulations of the BSC were computed by averaging 50 Monte Carlo realizations.

The influence of the relative permittivity of the medium on the BSC are shown in Figs. 4 and 5, where cases A, B and C are all considered. Figures 4(a) and 5(a) show the properties of ε_1, where $\varepsilon_2 = (9.8, 1.2)$. It is clear that the BSC from the lossless medium is larger than that of the lossy medium, and the BSC decreases as the imaginary part of ε_1 increases over the most scattering angles. We attribute this result to the fact that the imaginary part of a medium affects its absorption, with an increase of the imaginary part, the absorption becomes stronger and the reflectivity weakens, which leads a decrease of the BSC. In Figs. 4(b) and 5(b), the influences of ε_2 on the BSC are shown,

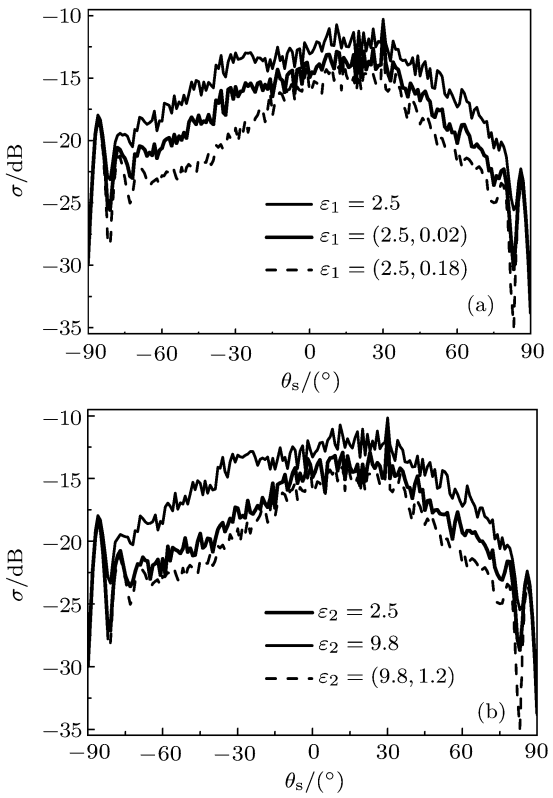


Fig. 4. BSC of case A for different ε_1 and ε_2 ($d_2 = 5\lambda$, $r = \lambda$, $z_p = 3\lambda$). (a) For different ε_1, (b) for different ε_2.

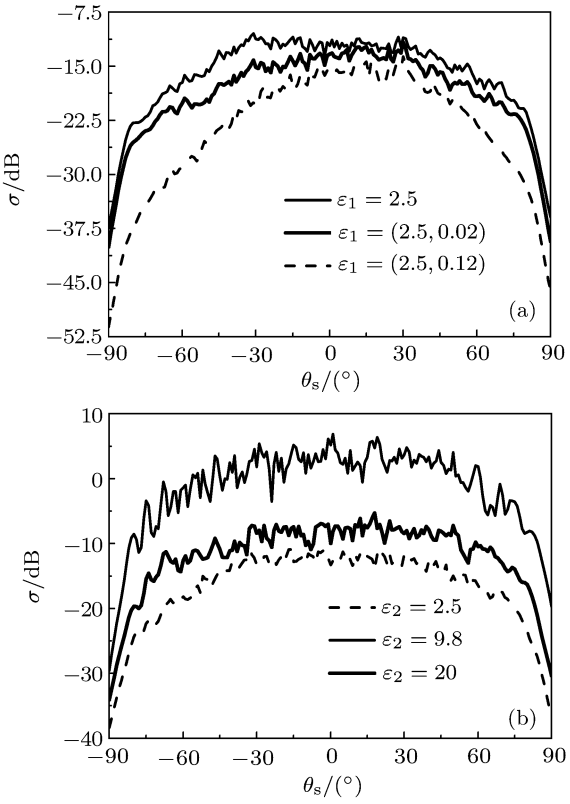


Fig. 5. BSC of cases B and C for different ε_1 and ε_2. (a) Case B for different ε_1 ($d_2 = 5\lambda$, $r = \lambda$, $z_p = -3\lambda$); (b) case C for different ε_2, ($d_2 = 2\lambda$, $r = \lambda$, $z_p = -5\lambda$).

in which $\varepsilon_1 = 2.5$. From Fig. 5(b), it is clear that the BSC is smallest for $\varepsilon_1 = \varepsilon_2 = 2.5$. A similar conclusion has been obtained by us in Ref. [3] through the FDTD technique.

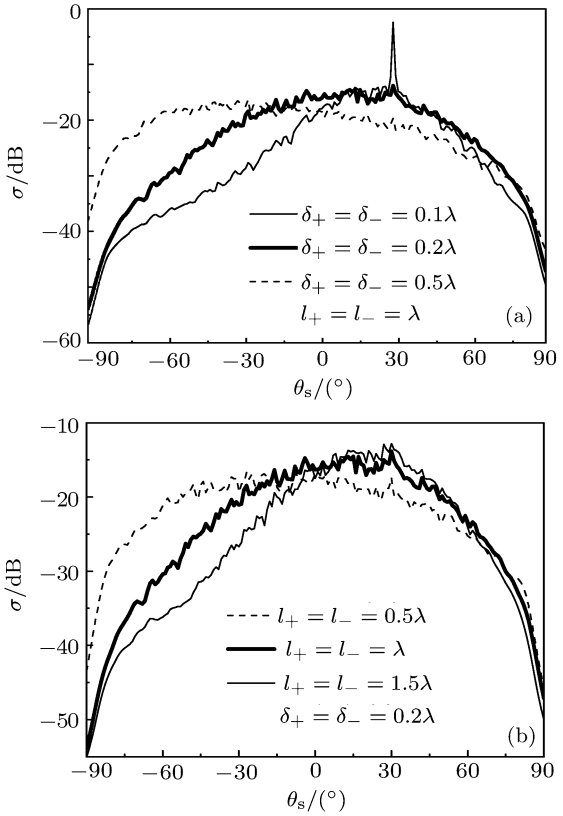


Fig. 6. BSC of case B for different δ and l ($d_2 = 5\lambda$, $r = \lambda$, $z_p = -3\lambda$). (a) For different δ, (b) for different l.

Figure 6 shows the dependences of the parameters of the Gaussian rough surface on the BSC of case B, including the rms height δ and the correlation length l. The relative permittivities were set to be $\varepsilon_1 = (2.5, 0.18)$ and $\varepsilon_2 = (9.8, 1.2)$, corresponding to soils with 3.8% moisture and 25% moisture, respectively.[21] The cylinder was located at $z_p = -3\lambda$ with $r = \lambda$ and $d_2 = 5\lambda$. From Fig. 6(a), it is found that there is an obvious peak in the specular direction for smaller rms heights. The primary reason for this is due to the fact that the roughness of the Gaussian rough surface depends on the rms height, the smaller the rms height, the smoother the Gaussian rough surface will be, leading to the obvious peak in the specular direction. Figure 6(b) presents the dependence of the BSC on correlation length. The BSC decreases with an increase of correlation length in the non-specular direction. This phenomenon mainly results from the fact that for smaller correlation lengths, the height fluctuation of Gaussian rough surface becomes more significant, which causes a more incoherent scattering contribution to the BSC. Similar conclusions have been obtained for cases A and C in Refs. [19] and [20].

Figure 7 shows the properties of the variation in the BSC of case B with the radius r and the altitude z_p of the cylinder. It is found that the BSC increases with the increasing radius, and decreases with the increasing altitude, especially for in the non-specular direction. This behavior can be attributed to the fact that the interactions are strengthened as the coupling area between the cylinder and the rough surface becomes larger with increasing radius or decreasing altitude, which causes the increasing BSC. This result is similar to that of an object above a single-layered rough surface obtained by our previous work.[10] From Fig. 7, it is also found that the scattering pattern of case B is greater than that of layered rough surface only (without object). Another point should be noted is that the BSC of case B without an object is nearly identical in the specular direction, which indicates that the coherent scattering in the specular direction depends more on the rough surfaces under these conditions.

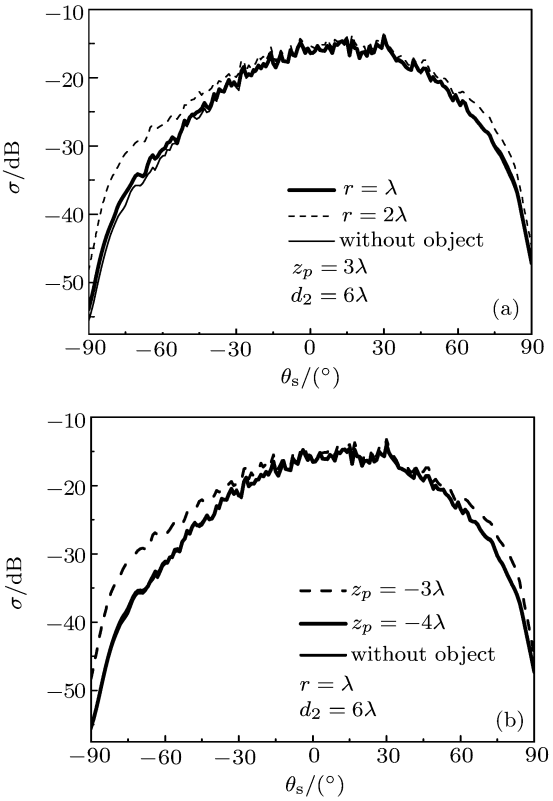


Fig. 7. BSC of case B for different r and z_p ($\varepsilon_1 = (2.5, 0.18)$, $\varepsilon_2 = (9.8, 1.2)$). (a) For different r, (b) for different z_p.

The effect of the average height d_2 between the two-layered rough surfaces on the BSC is also exam-

ined in Figs. 8 and 9. Comparing the two figures of Fig. 8, we can find that the BSC of the lossless medium is more affected by the average height. In other words, influences of the average height at the lossless case become more significant. Hence, in Fig. 9, only a lossless medium is considered. It is observed that the BSC changes very little with different heights for both cases B and C. The BSC is not "sensitive" to the variation of the average height d_2 under these two computational conditions.

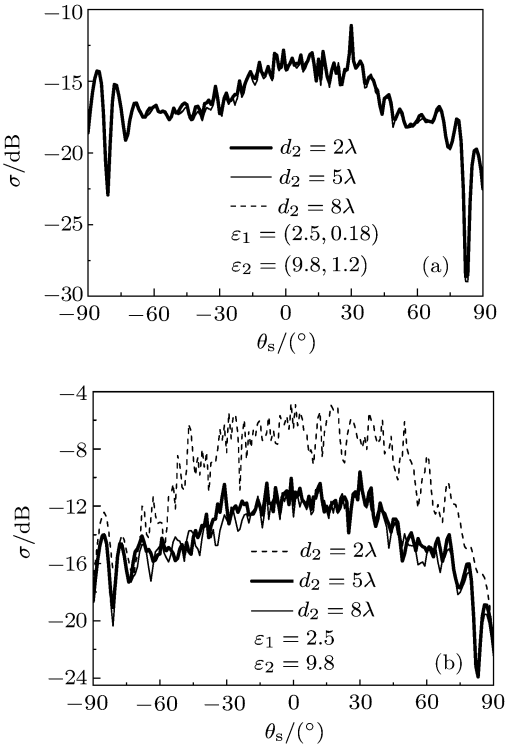


Fig. 8. BSC of case A with different d_2 ($r = \lambda$, $z_p = 3\lambda$). (a) Loss, (b) lossless.

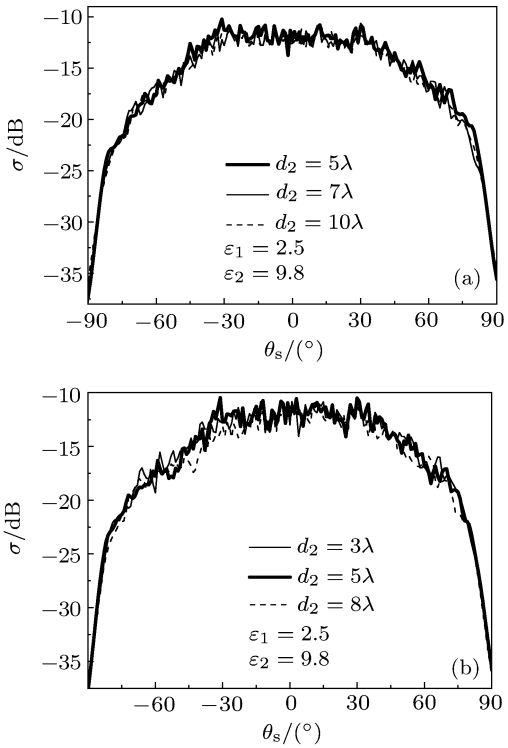


Fig. 9. BSC of case B and case C with different d_2. (a) case B ($r = \lambda$, $z_p = -3\alpha$), (b) case C ($r = \lambda$, $z_p = -10\alpha$).

4. Conclusions

In this study, EM scattering from two-layered rough interfaces with a PEC object under VV incidence were investigated through the MOM. Theoretical formulations, including integral equations and the matrix equations of EM scattering from multi-layered rough interfaces with a PEC object have been provided in detail. The two-layered scattering model is a special case. The validity of this study is proved by comparing it with existing solutions from previous literature.[6,18] The BSC is the smallest with the same medium, and the BSC of the lossless medium is larger than that of the lossy medium. It is necessary to point out that only VV polarization is considered in this study. The integral equations and the matrix equations for the horizontal case are different from those of the vertical case presented in this paper. In a further work, the MOM algorithm will be developed to solve this scattering problem under horizontal incidence. In addition, fast and advanced numerical methods, such as the fast multipole method[22] or the parallel MOM algorithm[9,10] will be introduced to study these scattering problems.

References

[1] Wang R, Guo L X and Ma J 2009 *Chin. Phys.* B **18** 3422

[2] Ren X C and Guo L X 2008 *Chin. Phys.* B **17** 2491

[3] Li J, Guo L X and Zeng H 2008 *Progress in Electromagnetics Research* **88** 197

[4] Kuo C H and Moghaddam M 2006 *IEEE Trans. Antennas Propagat.* **54** 2392

[5] Kuo C H and Moghaddam M 2008 *IEEE Trans. Antennas Propagat.* **56** 1133

[6] Déchamps N, Beaucoudrey N, Bourlier C and Toutain S 2006 *J. Opt. Soc. Am.* A **23** 359

[7] Déchamps N and Bourlier C 2007 *IEEE Trans. Antennas Propagat.* **55** 2790

[8] Kubické G, Bourlier C and Saillard J 2008 *Waves in Random and Complex Media* **18** 495

[9] Ma J, Guo L X and Wang A Q 2009 *Chin. Phys.* B **18** 3431

[10] Guo L X, Wang A Q and Ma J 2009 *Progress in Electromagnetics Research, PIER* **89** 149

[11] Wang A Q, Guo L X and Chai C 2010 *J. Electromagnetic Waves and Applications* **24** 1315

[12] Wang R, Guo L X, Ma J and Wu Z S 2009 *Chin. Phys.* B **18** 1503

[13] Li J, Guo L X, Zeng H and Han X B 2009 *Chin. Phys.* B **18** 2757

[14] Harrington R F 1993 *Field Computation by Moment Method* (New York: IEEE Press)

[15] Tsang L, Kong J A and Ding K H 2001 *Scattering of Electromagnetic Wave* (New York: John Wiley & Sons. Inc)

[16] Kelley C T 1995 *Iterative Methods for Linear and Nonlinear Equations* (Philadelphia: Society for Industrial and Applied Mathematics)

[17] Thorsos E I 1988 *Journal of Acoustical Society of American* **83** 78

[18] Wang X D, Wang C F, Gan Y B and Li L W 2003 *Progress in Electromagnetics Research* **40** 207

[19] Wang A Q, Guo L X and Chai C 2010 *Asia-Pacific International Symposium on Electromagnetic Compatibility* Beijing, April 12–16, 2010, p. 498

[20] Wang A Q, Guo L X and Chai C 2010 *Progress in Electromagnetics Research Symposium* March 22–26, 2010, p. 1028

[21] Curtis J 1996 *Dielectric Properties of Soils: Various Sites in Bosnia* (U.S. Army Corp. Eng., Washington, DC, Waterways Experim., Station Data Rep.)

[22] Lu C C and Chew W C 1993 *IEE Proceedings-H* **140** 455